Revised Submission to Geophysical Research Letters
Version 12

Cosmogenic $^{26}Al/^{10}Be$ Surface Production Ratio in Greenland

Lee B. Corbett*[a], Paul R. Bierman[a], Dylan H. Rood[b], Marc W. Caffee[c,d], Nathaniel A. Lifton[d,c], and Thomas E. Woodruff[c]

Total length = #words/500 + #tables + #figures
Length limit = 12 publication units
Current length = 7.99 + 1 + 3 = 11.99 publication units

*Corresponding Author: Ashley.Corbett@uvm.edu, (802) 380-2344
[a]Department of Geology, University of Vermont, Burlington, VT 05405
[b]Department of Earth Science and Engineering, Imperial College London, South Kensington Campus, London SW7 2AZ, UK
[c]Department of Physics and Astronomy, Purdue University, West Lafayette IN 47907
[d]Department of Earth, Atmospheric, and Planetary Sciences, Purdue University, West Lafayette IN 47907

Abstract

The assumed value for the cosmogenic $^{26}Al/^{10}Be$ surface production rate ratio in quartz is an important parameter for studies investigating the burial or subaerial erosion of long-lived surfaces and sediments. Recent models and data suggest that the production ratio is spatially variable and may be greater than originally thought. Here, we present measured $^{26}Al/^{10}Be$ ratios for 24 continuously exposed bedrock and boulder surfaces spanning ~61-77 °N in Greenland. Empirical measurements, such as ours, include nuclides produced predominately by neutron-induced spallation with percent-level contributions by muon interactions. The slope of a York regression line fit to our data is 7.3 ± 0.3 (1σ), suggesting that the $^{26}Al/^{10}Be$ surface production ratio exceeds the commonly used value of 6.75, at least in the Arctic. A higher $^{26}Al/^{10}Be$ production ratio has implications for multi-nuclide cosmogenic isotope studies because it results in greater modeled burial durations and erosion rates.

Key words: Geochronology; cosmogenic nuclides; burial; Arctic; Pleistocene

1. Introduction

The measurement of multiple cosmogenic nuclides [*Granger et al.*, 2013; *Lal*, 1988; *Nishiizumi et al.*, 1993; *von Blanckenburg and Willenbring*, 2014] constrains the history of rock surfaces and sediments that have experienced burial [*Granger*, 2006] or long-lived subaerial weathering [*Klein et al.*, 1986; *Nishiizumi et al.*, 1986]. Pairing two nuclides with different half-lives, such as ^{10}Be (~1.4 Ma [*Chmeleff et al.*, 2010]) and ^{26}Al (~0.7 Ma [*Nishiizumi*, 2004]), can detect complex sample histories involving the exposure/burial of surfaces covered by non-erosive glacial ice [*Bierman et al.*, 1999; *Stroeven et al.*, 2002], estimate the timing of sediment burial [*Balco and Rovey*, 2008; *Granger*, 2014; *Granger and Muzikar*, 2001], and quantify the exposure/erosion history of long-lived surfaces [*Brook et al.*, 1995]. Most two-nuclide cosmogenic isotope studies compare the measured ^{26}Al/^{10}Be ratio in quartz-bearing sample material to a nominal ^{26}Al/^{10}Be ratio at production [*Nishiizumi et al.*, 1991]; a sample ^{26}Al/^{10}Be ratio below that of the production ratio indicates burial or prolonged exposure.

The value of the ^{26}Al/^{10}Be production ratio remains uncertain for several reasons. 1) ^{26}Al has been measured much less frequently than ^{10}Be at production rate calibration sites. 2) Standards used to normalize measured isotopic ratios, as well as the assumed half-life of ^{10}Be, have changed over time [*Nishiizumi et al.*, 2007], but the assumed values of these parameters were typically not reported in most early publications estimating the ^{26}Al/^{10}Be production ratio (Supporting Information Table S1). 3) Although both ^{26}Al and ^{10}Be are produced predominately by neutron-induced spallation, muon interactions also produce these nuclides with an apparently higher ^{26}Al/^{10}Be production ratio [*Heisinger et al.*, 2002]. Hence, the measured ^{26}Al/^{10}Be of a sample is a combination of spallogenic nuclides and muogenic nuclides from the current period of exposure, as well as inherited spallogenic and muogenic nuclides from previous periods of

exposure. 4) There are substantial challenges and uncertainties in estimating nuclide production ratios including accurate characterization of production cross sections at relevant neutron energies [*Caffee et al.*, 2013]. Together, these reasons have prevented the accurate determination of the $^{26}Al/^{10}Be$ surface production ratio and its variation over latitude and altitude.

Because the $^{26}Al/^{10}Be$ production ratio is a key parameter in two-isotope interpretive models, the possibility that this ratio depends on geographic factors limits the accuracy of the two-isotope approach. This is especially relevant in the Arctic, where considerable $^{26}Al/^{10}Be$ burial dating has been conducted. The two-isotope approach has been used in Greenland [*Beel et al.*, 2016; *Corbett et al.*, 2016c; *Corbett et al.*, 2013; *Håkansson et al.*, 2009; *Roberts et al.*, 2008; *Roberts et al.*, 2009], Baffin Island [*Bierman et al.*, 2001; *Bierman et al.*, 1999; *Briner et al.*, 2006; *Briner et al.*, 2003; *Corbett et al.*, 2016a; *Kaplan et al.*, 2001; *Margreth et al.*, 2016; *Miller et al.*, 2006], mainland Arctic Canada [*Marquette et al.*, 2004], and Scandinavia [*Harbor et al.*, 2006; *Stroeven et al.*, 2002] to constrain the complex history of surfaces preserved beneath non-erosive glacial ice.

Here, we measure the $^{26}Al/^{10}Be$ production ratio at high latitude (~61-77 °N) in 24 samples collected from continuously exposed bedrock and boulder surfaces at four sites in Greenland (Fig. 1). All of these sites were exposed during ice margin retreat at the end of the Last Glacial Maximum [*Bennike and Björck*, 2002; *Sinclair et al.*, 2016]. The goal of this work is to use a field- and laboratory-based approach to further constrain the $^{26}Al/^{10}Be$ ratio at high latitude.

2. Previous Constraints on the $^{26}Al/^{10}Be$ Surface Production Ratio

Several different approaches have been used to estimate the $^{26}Al/^{10}Be$ production ratio, including direct measurement in young samples, inferences from long-exposed samples assumed to be at a secular equilibrium between production and decay, and model calculations (Supporting Information Table S1). Here, we report the original findings from these studies, without correcting for changes in nominal standard values and the ^{10}Be half-life; in Table S1, we have attempted to scale the inferred $^{26}Al/^{10}Be$ production ratios to currently accepted values.

Based on empirical analysis of field samples (representing nuclides produced from both spallation and muons), *Klein et al.* [1986] inferred a production ratio of ~7 in Libyan desert glass (25 °N); *Nishiizumi et al.* [1989] obtained an average of 6.02 ± 0.44 (1σ) from quartz extracted from glacially-polished Sierra Nevada granite (38 °N); *Nishiizumi et al.* [1991] calculated ~6.2 from Antarctic bedrock (72 °S) while *Brown et al.* [1991] calculated 6.5 ± 1.3 (1σ) from Antarctic moraines (78 °S); *Larsen* [1996] measured 5.88 ± 1.02 (average, 1σ) in Laurentide Ice Sheet terminal moraine material (41 °N); *Kubik et al.* [1998] determined a ratio of 6.52 ± 0.43 (weighted mean, 1σ) in Austrian landslide deposits (47 °N); and *Nishiizumi et al.* [2005] calculated ~6.1 from alluvial fan deposits in Chile (27 °S). Modeling and experimental studies estimated the spallation ratio to be 6.11 [*Lal*, 1991], 7.1 [*Reedy et al.*, 1994], and 6.05 [*Masarik and Reedy*, 1995].

Although there is spread in the measured production ratios and no systematic spatial trend, most of the original findings described above were consistent with a surface $^{26}Al/^{10}Be$ production ratio of ~6.1, and *Lal* [1991] adopted this ratio. It was used extensively in cosmogenic isotope studies until a change in the assumed value of primary accelerator standards [*Nishiizumi et al.*, 2007], as well as updates to the ^{10}Be half-life [*Chmeleff et al.*, 2010], raised

130 the canonical $^{26}Al/^{10}Be$ surface spallation production ratio to ~6.75, which is the value that is
131 currently used in the CRONUS Earth online calculator [*Balco et al.*, 2008]. Recently, studies
132 have refined cosmogenic nuclide production rates for different latitudes and altitudes. However,
133 most measured only ^{10}Be, inferring ^{26}Al indirectly by use of the canonical spallogenic surface
134 production ratio of 6.75 [*Balco et al.*, 2009; *Briner et al.*, 2012; *Goehring et al.*, 2012; *Kaplan et*
135 *al.*, 2011; *Kelly et al.*, 2015; *Putnam et al.*, 2010; *Young et al.*, 2013a]. As such, these recent
136 studies do not provide additional constraint of the $^{26}Al/^{10}Be$ production ratio.
137 A spallogenic $^{26}Al/^{10}Be$ production ratio exceeding 6.75 is consistent with modeling
138 studies that investigated the latitude and/or altitude scaling of ^{10}Be and ^{26}Al independently
139 [*Argento et al.*, 2013; *Lifton et al.*, 2014]. *Argento et al.* [2013], focusing on the high latitudes,
140 modeled a spallogenic $^{26}Al/^{10}Be$ production ratio of ~7.0-7.1 for sea level (their Table 2) and
141 found a small decrease in production ratio with increasing altitude (their Fig. 6). A recent
142 nuclide-specific scaling model [*Lifton et al.*, 2014], based on analytical approximations of
143 physics-based atmospheric cosmic-ray fluxes similar to those used by *Argento et al.* [2013],
144 *Argento et al.* [2015a], and *Argento et al.* [2015b], found variation in the production ratio over
145 both latitude and altitude (their Fig. 8).
146 Using a more complete and refined representation of the physics involved, *Argento et al.*
147 [2015a] also concluded that the $^{26}Al/^{10}Be$ production ratio varies with atmospheric depth (their
148 Fig. 6), but inferred a spallogenic ratio of 6.7 at sea level and high latitude, and lower ratios with
149 increasing altitude. Because of the modeling refinements, they consider the 2015 results to
150 supersede those from 2013. But while *Argento et al.* [2015a] cite improvements in radiation
151 transport model physics in preferring the new results compared to those from 2013, they also
152 note that they may be overestimating the ^{10}Be production rate by about 10% based on

153 comparison with recent ^{10}Be calibration site data [*Phillips et al.*, 2016], making their quoted
154 ^{26}Al/^{10}Be production ratios underestimates. Given the different ^{26}Al and ^{10}Be excitation functions
155 and the spallogenic nucleon energy spectra for the atmospheric depths relevant for in situ
156 cosmogenic nuclide production, both *Argento et al.* [2015a] and *Lifton et al.* [2014] suggested
157 that nuclide-specific scaling for altitude and latitude is appropriate. The new CRONUScalc
158 online calculator [*Marrero et al.*, 2016; *Phillips et al.*, 2016] treats the two nuclides
159 independently in terms of production rate models and thus production ratios.
160 Accompanying the numerical models, samples from calibration sites associated with the
161 CRONUS-Earth project provide empirical constraint for the ^{26}Al/^{10}Be production ratio [*Phillips*
162 *et al.*, 2016]. Analytical results from CRONUS-Earth calibration samples presented in *Argento et*
163 *al.* [2013] suggest that the ^{26}Al/^{10}Be production ratio (including both spallogenic and muogenic
164 contributions) exceeds the canonical value of 6.75. Their Fig. 7 shows that low-altitude (<2000
165 m) samples from six different calibration sites have a mean and median ^{26}Al/^{10}Be ratio of 7.2 (1σ
166 = 0.4, interquartile range = 0.4, n = 25). Using data from selected CRONUS-Earth production
167 rate calibration sites, *Borchers et al.* [2016] document surface ^{26}Al/^{10}Be ratios for Promontory
168 Point, Utah (1598-1606 m a.s.l., 41 °N: mean = 6.5, median = 6.6, 1σ = 0.7, interquartile range =
169 0.8, n = 19) and Scotland (131-528 m a.s.l., 57 °N: mean = 7.3, median = 7.2, 1σ = 0.6,
170 interquartile range = 0.4, n = 18), suggesting that altitude and latitude may play important roles
171 in production ratio scaling. However, the latitude and altitude of the calibration sites may be
172 internally correlated, as CRONUS-Earth sample sites tended to follow the snowline, leading to
173 higher-altitude calibration sites at low-latitude and lower-altitude calibration sites at high
174 latitude.
175

176 **3. Study Design and Assumptions**

177 To assess the $^{26}Al/^{10}Be$ production ratio at high latitude, we present isotopic ratio data
178 from four sites in Greenland spanning ~61-77 °N and 50-724 m a.s.l. (Table 1, Fig. 1). Modeled
179 production rates, scaled for latitude and altitude with both the CRONUS Earth online calculator
180 [*Balco et al.*, 2008] and the CRONUScalc online calculator [*Marrero et al.*, 2016], are shown in
181 Supporting Information Table S2 for each sample site. According to the CRONUS Earth online
182 calculator [*Balco et al.*, 2008], muon production represents 3.5 ± 0.5 % of total ^{10}Be production
183 and 4.3 ± 0.6 % of total ^{26}Al production (average, 1SD). According to the CRONUScalc online
184 calculator [*Marrero et al.*, 2016], muon production represents 1.4 ± 0.2 % of total ^{10}Be
185 production and 1.9 ± 0.2 % of total ^{26}Al production (average, 1SD). Since the CRONUS Earth
186 online calculator [*Balco et al.*, 2008] assumes a global $^{26}Al/^{10}Be$ spallation production ratio of
187 6.75, the summed spallogenic/muogenic $^{26}Al/^{10}Be$ production ratios for our samples are 6.79-
188 6.82 (Table S2). Conversely, location-scaled production rates from the CRONUScalc online
189 calculator [*Marrero et al.*, 2016] yield summed spallogenic/muogenic $^{26}Al/^{10}Be$ production ratios
190 of 7.26-7.30 (Tables 1 and S2).

191 The two southern study sites (Narsarsuaq, ~61°N, *Nelson et al.* [2014]; and Ilulissat,
192 ~69°N, *Corbett et al.* [2011]) were investigated previously using only ^{10}Be. The depth of glacial
193 erosion has not been definitively determined, but the existence of streamlined and striated
194 bedrock, as well as many ^{10}Be exposure ages coincident with local radiocarbon chronologies
195 (especially in Ilulissat), argue that the depth of erosion was at least several meters, removing all
196 spallogenic nuclides from prior periods of exposure [*Corbett et al.*, 2011; *Cronauer et al.*, 2016;
197 *Kelley et al.*, 2013; *Nelson et al.*, 2014; *Young et al.*, 2013b; *Young et al.*, 2011]. For these two

198 sites, the Al sample fraction was archived after initial sample preparation; we recovered and
199 analyzed that archived material (19 samples in total) for this study.
200 The two northern study sites (Upernavik, ~73°N, *Corbett et al.* [2013]; and Thule,
201 ~77°N, *Corbett et al.* [2015] and *Corbett et al.* [2016c]) were previously investigated with paired
202 ^{26}Al and ^{10}Be, and we make use of a subset of those data. Upernavik is characterized by deeply-
203 eroded fjords separated by highlands preserved beneath non-erosive glacial ice; here, we include
204 only samples from low elevations in the fjords [*Corbett et al.*, 2013]. Thule experienced
205 heterogeneous subglacial erosion and its boulders contain varying amounts of nuclides inherited
206 from previous periods of exposure; here, we utilize only the boulders that have ^{10}Be exposure
207 ages coincident with radiocarbon estimates of deglaciation timing [*Corbett et al.*, 2015].
208 Although we are unable to determine the depth of erosion during the last glaciation, we
209 infer that it was at least several meters because inherited nuclide concentrations from previous
210 periods of exposure are demonstrably low in the sample surfaces included here. If any of the
211 samples do contain spallogenic nuclides from previous periods of exposure, the shorter half-life
212 of ^{26}Al would drive the ^{26}Al/^{10}Be ratio downward during times of burial. Therefore, the ^{26}Al/^{10}Be
213 production ratios we infer would represent underestimates.
214 We do not think it is likely that muogenic production has made an appreciable impact on
215 our inferred ^{26}Al/^{10}Be production ratio. Penetrating more deeply into Earth's surface, muons
216 [*Heisinger et al.*, 2002] produce ^{10}Be and ^{26}Al at rates that are only a few percent of spallation
217 production rates (Table S2). The ^{26}Al/^{10}Be muon production ratio is not well-constrained, but a
218 value of ~8.35 is used in the CRONUS Earth online calculator [*Balco et al.*, 2008] and ~9.75 in
219 the CRONUScalc online calculator [*Marrero et al.*, 2016] for the locations of our sample sites
220 (Table S2). Although the muogenic ^{26}Al/^{10}Be production ratio is higher than that of spallation,

nuclides produced by muons during the present interglacial period represent such a small fraction of total isotope production that their impact on the surface production ratio is minimal.

Inherited nuclides from muogenic production are also unlikely to be important. Muogenic nuclides from previous periods of exposure may exist in sample surfaces independent of subglacial erosion history because muons penetrate deeply, thus even efficient glacial erosion is incapable of stripping away all muon-produced nuclides [*Briner et al.*, 2016]. However, nuclides inherited from previous interglacial periods when our sample sites were ice-free would have experienced burial following initial exposure, lowering the $^{26}Al/^{10}Be$ ratio by radioactive decay.

4. Methods

All samples were prepared at the University of Vermont using standard procedures [*Corbett et al.*, 2016b]. Additions of ^{27}Al carrier (1000 μg mL^{-1} SPEX Al standard) were optimized to reach a total of ~1500-2500 μg Al in each sample based on quantification of native Al in purified quartz. We quantified total ^{27}Al in the samples immediately following digestion with inductively-coupled plasma optical emission spectrometry (ICP-OES) analysis of replicate aliquots using two emission lines (308.215 and 309.271 nm) and two internal standards (Ga and Y).

We recovered archived Al sample fractions from Narsarsuaq (n = 9) and Ilulissat (n = 10) in 2016 (Table 1); these samples, which were stored as Al hydroxide gels since 2011 (Ilulissat) and 2014 (Narsarsuaq), had dried fully despite being in capped centrifuge tubes. We reconstituted the pellets in heated 10% nitric acid and re-precipitated Al hydroxide at pH 8. To remove Mg, which forms an isobar that interferes with ^{26}Al analysis on the Purdue Rare Isotope Measurement (PRIME) Laboratory Accelerator Mass Spectrometer, we used a modified cation

chromatography method. Our standard Be elution (five column volumes of 1.2 N HCl, *Corbett et al.* [2016b]) was followed by a Mg elution (an additional eight column volumes of 1.2 N HCl) before elution of Al (four column volumes of 4N HCl). ICP-OES analysis of small aliquots from the samples after processing indicated that sample recovery was 75 ± 11 % (average, 1σ, n = 19) of the original total Al in the samples.

Isotope ratios (Supporting Information Table S3) reported in the original publications [*Corbett et al.*, 2016c; *Corbett et al.*, 2015; *Corbett et al.*, 2013; *Corbett et al.*, 2011; *Nelson et al.*, 2014] were measured by Accelerator Mass Spectrometry (AMS) at Lawrence Livermore National Laboratory ($^{10}Be/^{9}Be$ from Narsarsuaq, Ilulissat, and Upernavik, as well as $^{26}Al/^{27}Al$ from Upernavik) and Scottish Universities Environmental Research Centre ($^{10}Be/^{9}Be$ and $^{26}Al/^{27}Al$ from Thule). Isotope ratios for the new $^{26}Al/^{27}Al$ data reported here were measured at PRIME Laboratory. For the new $^{26}Al/^{27}Al$ analyses from Narsarsuaq and Ilulissat (Supporting Information Table S3), ICP-quantified total Al ranged from 1433-3115 μg. Sample ratios were normalized to standard KNSTD with an assumed ratio of 1.818×10^{-12} [*Nishiizumi*, 2004]. Measured ratios for the new ^{26}Al analyses (n = 19) ranged from 6.2 to 41.2 x 10^{-14}, and analytic uncertainties were 4.8 ± 1.4 % (average, 1σ).

Measured $^{26}Al/^{27}Al$ ratios for process blanks (n = 6; Supporting Information Table S4 and Fig. S1) at PRIME Laboratory were scattered, with four blanks yielding low, indistinguishable ratios averaging 7.7×10^{-16} and the remaining two blanks almost an order of magnitude higher with ratios of 6.1×10^{-15} (from the Ilulissat study) and 7.5×10^{-15} (from the Narsarsuaq study). We chose to discard the high ^{26}Al blank from the Narsarsuaq study since it was discarded in the original publication of the ^{10}Be data, where it was the only elevated blank of nine that were measured [*Nelson et al.*, 2014].

To account for multiple possible blank corrections for the new ^{26}Al PRIME Laboratory measurements, we performed a sensitivity analysis utilizing four different backgrounds (Supporting Information Table S5): mean or median blank value with the high Ilulissat blank included or excluded. All four possibilities use one standard deviation around the mean to propagate blank uncertainty into the sample uncertainties in quadrature. The sensitivity analysis demonstrates that the choice of blank correction is insignificant; calculated ^{26}Al/^{10}Be ratios vary by only 0.06 ± 0.04 across all four scenarios, resulting in a 0.8 ± 0.5 % difference (n = 19, average, 1σ). For the new ^{26}Al analyses presented in this manuscript, we chose to use the median blank value (without discarding the high Ilulissat blank) and one standard deviation around the mean, which yields a ^{26}Al/^{27}Al background of 6.9 ± 24.6 x10^{-16}. We subtracted the blank ratio from all samples and propagated uncertainties in quadrature; this blank represents a 0.2 - 1.1 % (average 0.4 ± 0.2 %, 1σ) correction of the sample ratios. The ^{26}Al concentrations and ^{26}Al/^{10}Be ratios for the four possible blank corrections are shown in the Supporting Information (Table S5).

5. Results

Our measurements of stable ^{27}Al, an important part of quantifying ^{26}Al, are robust. For the blanks included in the ten batches of samples described here, the expected (as determined through the addition of ^{27}Al carrier) and the measured (as determined through ICP-OES analysis) Al contents differ by only 2.0 ± 2.4 % (absolute value, n = 13, 1σ). This indicates that ICP-OES quantification of total Al in samples is accurate, with little or no loss of Al through precipitation of fluoride compounds [*Bierman and Caffee*, 2002]. The long-term calculated ^{26}Al concentration of the quality control material CRONUS-N in the University of Vermont Laboratory is 1.03 ±

290 0.05 x10^6 atoms g^{-1} (average, n = 13, 1σ), which is indistinguishable from the value of 1.05 ±
291 0.11 x10^6 atoms g^{-1} (n = 10, 1σ) obtained by *Jull et al.* [2015].

292 Across the dataset as a whole, blank-corrected sample ^{10}Be concentrations range from 3.5
293 – 9.1 x10^4 atoms g^{-1} and ^{26}Al concentrations range from 2.6 – 6.4 x10^5 atoms g^{-1} (n = 24, Table
294 1). Calculated ^{26}Al/^{10}Be ratios are 6.07 – 8.42, with uncertainties of 5.8 ± 2.0 % (n = 24, average,
295 1σ; Table 1). However, the lowest calculated ^{26}Al/^{10}Be ratio (GLX25A, 6.07 ± 0.25) is >2σ
296 below the dataset mean and is a statistical outlier using Peirce's Criterion; we therefore infer that
297 this sample likely records a complex history and omit it from our further calculations.

298 After omission of sample GLX25A, the calculated ^{26}Al/^{10}Be ratios range from 6.79 to
299 8.42 (n = 23, Table 1, Fig. 2). The arithmetic mean ^{26}Al/^{10}Be ratio for the entire dataset is 7.4 ±
300 0.5 (n = 23, 1σ). The median, similar to the mean, is 7.3, and the interquartile range is 0.6. The
301 direct uncertainty-weighted mean is 7.3 ± 0.1 (1σ). A York regression, which accounts for
302 uncertainties in both ^{10}Be and ^{26}Al, gives a slope (i.e. ^{26}Al/^{10}Be ratio) of 7.3 ± 0.3 (1σ) and a y-
303 intercept that is statistically indistinguishable from zero at 1σ (Fig. 3). There is no statistically-
304 significant spatial variability of ^{26}Al/^{10}Be ratio within the limited latitude/altitude range of the
305 study area, consistent with theoretical predictions [*Argento et al.*, 2013; *Argento et al.*, 2015b;
306 *Lifton et al.*, 2014]; sample ^{26}Al/^{10}Be ratios are not significantly correlated with latitude (R^2 =
307 0.03, p = 0.39) or altitude (R^2 = 0.03, p = 0.41), nor are they separable by site (p = 0.80 using a
308 one-way analysis of variance).

309

310 **6. Discussion**

311 Analysis of paired ^{26}Al/^{10}Be data from continuously exposed samples in Greenland
312 indicates that the high latitude, low altitude ^{26}Al/^{10}Be surface production ratio in quartz,

313 incorporating both spallation and muon interactions, is 7.3 ± 0.3 (slope of a York regression, 1σ,
314 Fig. 3). Assuming a muon contribution of 1.5%, a muogenic $^{26}Al/^{10}Be$ production ratio of 9.75
315 [*Marrero et al.*, 2016], and a summed spallogenic/muogenic $^{26}Al/^{10}Be$ production ratio of 7.3,
316 we calculate a spallation-only $^{26}Al/^{10}Be$ production ratio of 7.25. This value is about 8% higher
317 than the currently accepted spallation value of 6.75 ± 0.5 (based on *Nishiizumi et al.* [1986],
318 normalized to standard values presented in *Nishiizumi et al.* [2007]).
319 It seems unlikely that analytic uncertainties alone explain the differences in the measured
320 production ratios; rather, we suggest that latitude dependence or other site-specific factors
321 control the production ratio. A production ratio exceeding 6.75 is consistent with other studies
322 that investigated the scaling of ^{10}Be and ^{26}Al independently, especially the values presented in
323 *Argento et al.* [2013] and *Lifton et al.* [2014]. The production ratio we calculate here exceeds the
324 value of ~6.7 that *Argento et al.* [2015b] inferred for sea level and high latitude, which is more
325 consistent with the canonical value. However, the findings of *Argento et al.* [2015b] may be
326 biased by a ^{10}Be production rate that is ~10% too high; correcting the ^{10}Be production rate
327 downward, their inferred $^{26}Al/^{10}Be$ production ratio is ~7.4, which aligns closely with the value
328 we determined in Greenland. The production ratio we measure here agrees with site-specific
329 production ratios (Tables 1 and S2) calculated using the CRONUScalc online calculator
330 [*Marrero et al.*, 2016] and "SA" scaling [*Lifton et al.*, 2014].
331 Available published data are not sufficient to fully evaluate the scaling of the $^{26}Al/^{10}Be$
332 production ratio over space due to two key limitations. First, in the past, ^{26}Al measurements
333 typically had greater statistical uncertainties than ^{10}Be measurements, yielding low-precision
334 $^{26}Al/^{10}Be$ ratios. Second, no systematic studies with high-precision measurements have been
335 conducted in which the production ratios were measured in a suite of samples where only one

336 geographic parameter (latitude for example) varied. Such studies are needed to clarify the
337 $^{26}Al/^{10}Be$ production ratio at different latitudes and altitudes.

338 The $^{26}Al/^{10}Be$ surface production ratio in quartz has important implications for the
339 histories inferred using cosmogenic nuclide analysis in bedrock and boulder surfaces. A higher
340 than currently accepted $^{26}Al/^{10}Be$ production ratio would result in more samples that record a
341 history of burial and longer modeled burial durations. As demonstrated by a sensitivity analysis
342 in *Corbett et al.* [2016c], an assumed $^{26}Al/^{10}Be$ production ratio of 7.35 results in the conclusion
343 that 61% of boulders in the dataset experienced burial, whereas an assumed production ratio of
344 6.75 suggests that only 21% of boulders have been buried (where burial is defined by a sample
345 point falling >1σ below the constant production or steady erosion curve). Further, for every 0.1
346 increase in assumed production ratio, modeled burial durations for a representative sample in
347 *Corbett et al.* [2016c] increased by 53 ky. Thus the change we suggest here (from 6.75 to 7.3)
348 would increase burial ages by nearly 300 ky.
349

350 **7. Conclusions**

351 Analysis of continuously exposed quartz-bearing bedrock and boulder surfaces spanning
352 ~61-77 °N in Greenland yields a surface $^{26}Al/^{10}Be$ production ratio of 7.3 ± 0.3 (slope of a York
353 regression, 1σ, spallation and muons). The surfaces we analyzed here were eroded during the last
354 glaciation, appear to have simple exposure histories (excluding one outlier), and have been
355 exposed since ice retreated across the landscape at the beginning of the Holocene. The $^{26}Al/^{10}Be$
356 ratio we determine is ~8% greater than that used for most studies, suggesting that the canonical
357 production ratio is not appropriate for at least certain areas of the world, perhaps because
358 production rates of these two cosmogenic nuclides do not scale similarly over space. Since most

two-isotope cosmogenic studies rely on the $^{26}Al/^{10}Be$ surface production ratio as a central assumption, this new constraint on the ratio has important implications for inferred exposure, burial, and erosion histories, especially in the Arctic. Our results suggest that additional production ratio calibrations are necessary globally.

Acknowledgements

Funding was provided by NSF ARC-0713956 and NSF ARC-1023191 to Bierman and NSF BCS-1433878 to Corbett. Corbett was also supported by an NSF Graduate Research Fellowship and grants from Geological Society of America Quaternary Geology and Geomorphology Division J. Hoover Mackin Award and the International Association of Geochemistry. We thank CH2MHILL Polar Services for support during fieldwork. MWC and TEW acknowledge support from NSF EAR-0919759; NAL acknowledges support from NSF EAR-1560658. D. Argento and one anonymous reviewer provided suggestions that improved the manuscript. Data from this study are available in Table 1 as well as Tables S1 through S5 of the Supporting Information.

References

Argento, D., R. Reedy, and J. Stone (2013), Modeling the earth's cosmic radiation, *Nuclear Instruments and Methods in Physics Research B*, *294*, 464-469.

Argento, D., J. Stone, R. Reedy, and K. O'Brien (2015a), Physics-based modeling of cosmogenic nuclides part I–radiation transport methods and new insights, *Quaternary Geochronology*, *26*, 29-43.

Argento, D., J. Stone, R. Reedy, and K. O'Brien (2015b), Physics-based modeling of cosmogenic nuclides part II- Key aspects of in-situ cosmogenic nuclide production, *Quaternary Geochronology*, *26*, 44-55.

Balco, G., and C. Rovey (2008), An isochron method for cosmogenic-nuclide dating of buried soils and sediments, *American Journal of Science*, *308*, 1083-1114.

Balco, G., J. Stone, N. Lifton, and T. Dunai (2008), A complete and easily accessible means of calculating surface exposure ages or erosion rates from ^{10}Be and ^{26}Al measurements, *Quaternary Geochronology*, *3*(3), 174-195.

Balco, G., J. Briner, R. Finkel, J. Rayburn, J. Ridge, and J. Schaefer (2009), Regional beryllium-10 production rate calibration for late-glacial northeastern North America, *Quaternary Geochronology*, *4*(2), 93-107.

Beel, C., N. Lifton, J. Briner, and B. Goehring (2016), Quaternary evolution and ice sheet history of contrasting landscapes in Uummannaq and Sukkertoppen, western Greenland, *Quaternary Science Reviews*, *149*, 248-258.

Bennike, O., and S. Björck (2002), Chronology of the last recession of the Greenland Ice Sheet, *Journal of Quaternary Science*, *17*(3), 211-219.

Bierman, P., and M. Caffee (2002), Cosmogenic exposure and erosion history of Australian bedrock landforms, *Bulletin of the Geological Society of America*, *114*(7), 787-803.

Bierman, P., K. Marsella, P. Davis, and M. Caffee (2001), Response to Discussion by Wolfe et al. on Bierman et al. (Geomorphology 25 (1999) 25–39), *Geomorphology*, *39*, 255-260.

Bierman, P., K. Marsella, C. Patterson, P. Davis, and M. Caffee (1999), Mid-Pleistocene cosmogenic minimum-age limits for pre-Wisconsinan glacial surfaces in southwestern Minnesota and southern Baffin Island: a multiple nuclide approach, *Geomorphology*, *27*(1), 25-39.

Borchers, B., S. Marrero, G. Balco, M. Caffee, B. Goehring, N. Lifton, K. Nishiizumi, F. Phillips, J. Schaefer, and J. Stone (2016), Geological calibration of spallation production rates in the CRONUS-Earth project, *Quaternary Geochronology*, *31*, 188-198.

Briner, J., G. Miller, P. Davis, and R. Finkel (2006), Cosmogenic radionuclides from fjord landscapes support differential erosion by overriding ice sheets, *Geological Society of America Bulletin*, *118*(3/4), 406-420.

Briner, J., N. Young, B. Goehring, and J. Schaefer (2012), Constraining Holocene ^{10}Be production rates in Greenland, *Journal of Quaternary Science*, *27*(1), 2-6.

Briner, J., B. Goehring, J. Mangerud, and J. Svendsen (2016), The deep accumulation of 10Be at Utsira, southwestern Norway: Implications for cosmogenic nuclide exposure dating in peripheral ice sheet landscapes, *Geophysical Research Letters*, *43*(17), 9121-9129.

Briner, J., G. Miller, P. Davis, P. Bierman, and M. Caffee (2003), Last Glacial Maximum ice sheet dynamics in Arctic Canada inferred from young erratics perched on ancient tors, *Quaternary Science Reviews*, *22*(5-7), 437-444.

Brook, E., E. Brown, M. Kurz, R. Ackert, G. Raisbeck, and F. Yiou (1995), Constraints on age, erosion, and uplift of Neogene glacial deposits in the Transantarctic Mountains determined from in situ cosmogenic ^{10}Be and ^{26}Al, *Geology*, *23*(12), 1063-1066.

Brown, E., J. Edmond, G. Raisbeck, F. Yiou, M. Kurz, and E. Brook (1991), Examination of surface exposure ages of Antarctic moraines using in situ produced ^{10}Be and ^{26}Al, *Geochimica et Cosmochimica Acta*, *55*(8), 2269-2283.

Caffee, M., K. Nishiizumi, J. Sisterson, J. Ullmann, and K. Welten (2013), Cross section measurements at neutron energies 71 and 112MeV and energy integrated cross section measurements ($0.1 < E_n < 750$ MeV) for the neutron induced reactions O(n, x)^{10}Be, Si(n, x)^{10}Be, and Si(n, x)^{26}Al, *Nuclear Instruments and Methods in Physics Research Section B: Beam Interactions with Materials and Atoms*, *294*, 479-483.

Chmeleff, J., F. Von Blanckenburg, K. Kossert, and D. Jakob (2010), Determination of the ^{10}Be half-life by multicollector ICP-MS and liquid scintillation counting, *Nuclear Instruments and Methods in Physics Research Section B: Beam Interactions with Materials and Atoms*, *268*(2), 192-199.

Corbett, L., P. Bierman, and P. Davis (2016a), Glacial history and landscape evolution of southern Cumberland Peninsula, Baffin Island, Canada, constrained by cosmogenic ^{10}Be and ^{26}Al, *Geological Society of America Bulletin*, *128*, 1173-1192.

Corbett, L., P. Bierman, and D. Rood (2016b), An approach for optimizing in situ cosmogenic ^{10}Be sample preparation, *Quaternary Geochronology*, *33*, 24-34.

Corbett, L., P. Bierman, and D. Rood (2016c), Constraining multi-stage exposure-burial scenarios for boulders preserved beneath cold-based glacial ice in Thule, northwest Greenland, *Earth and Planetary Science Letters*, *440*, 147-157.

Corbett, L., P. Bierman, G. Lasher, and D. Rood (2015), Landscape chronology and glacial history in Thule, northwest Greenland, *Quaternary Science Reviews*, *109*, 57-67.

Corbett, L., P. Bierman, J. Graly, T. Neumann, and D. Rood (2013), Constraining landscape history and glacial erosivity using paired cosmogenic nuclides in Upernavik, northwest Greenland, *Geological Society of America Bulletin*, *125*(9/10), 1539-1553.

Corbett, L., N. Young, P. Bierman, J. Briner, T. Neumann, J. Graly, and D. Rood (2011), Paired bedrock and boulder ^{10}Be concentrations resulting from early Holocene ice retreat near Jakobshavn Isfjord, western Greenland, *Quaternary Science Reviews*, *30*, 1739-1749.

Cronauer, S., J. Briner, S. Kellet, S. Zimmerman, and M. Morlighem (2016), ^{10}Be dating reveals early-middle Holocene age of the Drygalski moraines in central west Greenland, *Quaternary Science Reviews*, *147*, 59-68.

Goehring, B., Ø. Lohne, J. Mangerud, J. Svendsen, R. Gyllencreutz, J. Schaefer, and R. Finkel (2012), Late glacial and holocene ^{10}Be production rates for western Norway, *Journal of Quaternary Science*, *27*(1), 89-96.

Granger, D. (2006), A review of burial dating methods using ^{26}Al and ^{10}Be, *Geological Society of America Special Papers*, *415*, 1-16.

Granger, D. (2014), Cosmogenic nuclide burial dating in archaeology and paleoanthropology, in *Treatise on Geochemistry*, edited by H. Holland and K. Turekian, pp. 81-97, Elsevier.

Granger, D., and P. Muzikar (2001), Dating sediment burial with in situ-produced cosmogenic nuclides: theory, techniques, and limitations, *Earth and Planetary Science Letters*, *188*(1-2), 269-281.

460 Granger, D., N. Lifton, and J. Willenbring (2013), A cosmic trip: 25 years of cosmogenic
461 nuclides in geology, *Geological Society of America Bulletin*, *125*(9-10), 1379-1402.
462 Håkansson, L., H. Alexanderson, C. Hjort, P. Moller, J. Briner, A. Aldahan, and G. Possnert
463 (2009), Late Pleistocene glacial history of Jameson Land, central East Greenland, derived
464 from cosmogenic ^{10}Be and ^{26}Al exposure dating, *Boreas*, *38*(2), 244-260.
465 Harbor, J., A. Stroeven, D. Fabel, A. Clarhäll, J. Kleman, Y. Li, D. Elmore, and D. Fink (2006),
466 Cosmogenic nuclide evidence for minimal erosion across two subglacial sliding
467 boundaries of the late glacial Fennoscandian ice sheet, *Geomorphology*, *75*(1-2), 90-99.
468 Heisinger, B., D. Lal, A. Jull, P. Kubik, S. Ivy-Ochs, S. Neumaier, K. Knie, V. Lazarev, and E.
469 Nolte (2002), Production of selected cosmogenic radionuclides by muons: 1. Fast muons,
470 *Earth and Planetary Science Letters*, *200*(3-4), 345-355.
471 Jull, A., E. Scott, and P. Bierman (2015), The CRONUS-Earth inter-comparison for cosmogenic
472 isotope analysis, *Quaternary Geochronology*, *26*, 3-10.
473 Kaplan, M., G. Miller, and E. Steig (2001), Low-gradient outlet glaciers (ice streams?) drained
474 the Laurentide ice sheet, *Geology*, *29*(4), 343-346.
475 Kaplan, M., J. Strelin, J. Schaefer, G. Denton, R. Finkel, R. Schwartz, A. Putnam, M.
476 Vandergoes, B. Goehring, and S. Travis (2011), In-situ cosmogenic ^{10}Be production rate
477 at Lago Argentino, Patagonia: implications for late-glacial climate chronology, *Earth and*
478 *Planetary Science Letters*, *309*(1), 21-32.
479 Kelley, S., J. Briner, and N. Young (2013), Rapid ice retreat in Disko Bugt supported by ^{10}Be
480 dating of the last recession of the western Greenland Ice Sheet, *Quaternary Science*
481 *Reviews*, *82*, 13-22.
482 Kelly, M., T. Lowell, P. Applegate, F. Phillips, J. Schaefer, C. Smith, H. Kim, K. Leonard, and
483 A. Hudson (2015), A locally calibrated, late glacial ^{10}Be production rate from a low-
484 latitude, high-altitude site in the Peruvian Andes, *Quaternary Geochronology*, *26*, 70-85.
485 Klein, J., R. Giegengack, R. Middleton, P. Sharma, J. Underwood, and R. Weeks (1986),
486 Revealing histories of exposure using *in situ* produced ^{26}Al and ^{10}Be in Libyan desert
487 glass, *Radiocarbon*, *28*(2A), 547-555.
488 Kubik, P., S. Ivy-Ochs, J. Masarik, M. Frank, and C. Schluchter (1998), ^{10}Be and ^{26}Al production
489 rates deduced from an instantaneous event within the dendro-calibration curve, the
490 landslide of Kofels, Otz Valley, Austria, *Earth and Planetary Science Letters*, *161*, 231-
491 241.
492 Lal, D. (1988), In situ-produced cosmogenic isotopes in terrestrial rocks, *Annual Review of Earth*
493 *and Planetary Sciences*, *16*(1), 355-388.
494 Lal, D. (1991), Cosmic ray labeling of erosion surfaces: in situ nuclide production rates and
495 erosion models, *Earth and Planetary Science Letters*, *104*(2-4), 424-439.
496 Larsen, P. (1996), In-situ production rates of cosmogenic ^{10}Be and ^{26}Al over the past 21,500
497 years determined from the terminal moraine of the Laurentide Ice Sheet, North-Central
498 New Jersey, 142 pp, University of Vermont, Burlington, Vermont.
499 Lifton, N., T. Sato, and T. Dunai (2014), Scaling in situ cosmogenic nuclide production rates
500 using analytical approximations to atmospheric cosmic-ray fluxes, *Earth and Planetary*
501 *Science Letters*, *386*, 149-160.
502 Margreth, A., J. Gosse, and A. Dyke (2016), Quantification of subaerial and episodic subglacial
503 erosion rates on high latitude upland plateaus: Cumberland Peninsula, Baffin Island,
504 Arctic Canada, *Quaternary Science Reviews*, *133*, 108-129.

505 Marquette, G., J. Gray, J. Gosse, F. Courchesne, L. Stockli, G. Macpherson, and R. Finkel
506 (2004), Felsenmeer persistence under non-erosive ice in the Torngat and Kaumajet
507 mountains, Quebec and Labrador, as determined by soil weathering and cosmogenic
508 nuclide exposure dating, *Canadian Journal of Earth Sciences*, *41*(1), 19-38.
509 Marrero, S., F. Phillips, B. Borchers, N. Lifton, R. Aumer, and G. Balco (2016), Cosmogenic
510 nuclide systematics and the CRONUScalc program, *Quaternary Geochronology*, *31*, 160-
511 187.
512 Masarik, J., and R. Reedy (1995), Terrestrial cosmogenic-nuclide production systematics
513 calculated from numerical simulations, *Earth and Planetary Science Letters*, *136*(3), 381-
514 395.
515 Miller, G., J. Briner, N. Lifton, and R. Finkel (2006), Limited ice-sheet erosion and complex
516 exposure histories derived from in situ cosmogenic ^{10}Be, ^{26}Al, and ^{14}C on Baffin Island,
517 Arctic Canada, *Quaternary Geochronology*, *1*, 74-85.
518 Nelson, A., P. Bierman, J. Shakun, and D. Rood (2014), Using in situ cosmogenic ^{10}Be to
519 identify the source of sediment leaving Greenland, *Earth Surface Processes and*
520 *Landforms*, *39*, 1087-1100.
521 Nishiizumi, K. (2004), Preparation of ^{26}Al AMS standards, *Nuclear Instruments and Methods in*
522 *Physics Research Section B: Beam Interactions with Materials and Atoms*, *223-224*, 388-
523 392.
524 Nishiizumi, K., D. Lal, J. Klein, R. Middleton, and J. Arnold (1986), Production of ^{10}Be and ^{26}Al
525 by cosmic rays in terrestrial quartz in situ and implications for erosion rates, *Nature*, *319*,
526 134-136.
527 Nishiizumi, K., M. Caffee, R. Finkel, G. Brimhall, and T. Mote (2005), Remnants of a fossil
528 alluvial fan landscape of Miocene age in the Atacama Desert of northern Chile using
529 cosmogenic nuclide exposure age dating, *Earth and Planetary Science Letters*, *237*(3),
530 499-507.
531 Nishiizumi, K., C. Kohl, J. Arnold, J. Klein, D. Fink, and R. Middleton (1991), Cosmic ray
532 produced ^{10}Be and ^{26}Al in Antarctic rocks: exposure and erosion history, *Earth and*
533 *Planetary Science Letters*, *104*(2-4), 440-454.
534 Nishiizumi, K., M. Imamura, M. Caffee, J. Southon, R. Finkel, and J. McAninch (2007),
535 Absolute calibration of ^{10}Be AMS standards, *Nuclear Instruments and Methods in*
536 *Physics Research Section B: Beam Interactions with Materials and Atoms*, *258*(2), 403-
537 413.
538 Nishiizumi, K., E. Winterer, C. Kohl, J. Klein, R. Middleton, D. Lal, and J. Arnold (1989),
539 Cosmic ray production rates of ^{10}Be and ^{26}Al in quartz from glacially polished rocks,
540 *Journal of Geophysical Research*, *94*(B12), 17907.
541 Nishiizumi, K., C. Kohl, J. Arnold, R. Dorn, I. Klein, D. Fink, R. Middleton, and D. Lal (1993),
542 Role of in situ cosmogenic nuclides ^{10}Be and ^{26}Al in the study of diverse geomorphic
543 processes, *Earth Surface Processes and Landforms*, *18*(5), 407-425.
544 Phillips, F., et al. (2016), The CRONUS-Earth project: a synthesis, *Quaternary Geochronology*,
545 *31*, 119-154.
546 Putnam, A., J. Schaefer, D. Barrell, M. Vandergoes, G. Denton, M. Kaplan, R. Finkel, R.
547 Schwartz, B. Goehring, and S. Kelley (2010), In situ cosmogenic ^{10}Be production-rate
548 calibration from the Southern Alps, New Zealand, *Quaternary Geochronology*, *5*(4), 392-
549 409.

Reedy, R., K. Nishiizumi, D. Lal, J. Arnold, P. Englert, J. Klein, R. Middleton, A. Jull, and D. Donahue (1994), Simulations of terrestrial in-situ cosmogenic nuclide production, *Nuclear Instruments and Methods in Physics Research B*, *92*, 297-300.

Roberts, D., A. Long, C. Schnabel, S. Freeman, and M. Simpson (2008), The deglacial history of southeast sector of the Greenland Ice Sheet during the Last Glacial Maximum, *Quaternary Science Reviews*, *27*, 1505-1516.

Roberts, D., A. Long, C. Schnabel, B. Davies, S. Xu, M. Simpson, and P. Huybrechts (2009), Ice sheet extent and early deglacial history of the southwestern sector of the Greenland Ice Sheet, *Quaternary Science Reviews*, *28*, 2760-2773.

Sinclair, G., A. Carlson, A. Mix, B. Lecavalier, G. Milne, A. Mathias, C. Buizert, and R. DeConto (2016), Diachronous retreat of the Greenland ice sheet during the last deglaciation, *Quaternary Science Reviews*, *145*, 243-258.

Stroeven, A., D. Fabel, C. Hattestrand, and J. Harbor (2002), A relict landscape in the centre of Fennoscandian glaciation: cosmogenic radionuclide evidence of tors preserved through multiple glacial cycles, *Geomorphology*, *44*(1-2), 145-154.

von Blanckenburg, F., and J. Willenbring (2014), Cosmogenic nuclides: dates and rates of Earth-surface change, *Elements*, *10*(5), 341-346.

Young, N., J. Schaefer, J. Briner, and B. Goehring (2013a), A ^{10}Be production-rate calibration for the Arctic, *Journal of Quaternary Science*, *28*(5), 515-526.

Young, N., J. Briner, D. Rood, R. Finkel, L. Corbett, and P. Bierman (2013b), Age of the Fjord Stade moraines in the Disko Bugt region, western Greenland, and the 9.3 and 8.2 ka cooling events, *Quaternary Science Reviews*, *60*, 76-90.

Young, N., J. Briner, H. Stewart, Y. Axford, B. Csatho, D. Rood, and R. Finkel (2011), Response of Jakobshavn Isbrae, Greenland, to Holocene climate change, *Geology*, *39*(2), 131-134.

Table Captions

Table 1. Location and isotopic information for 24 bedrock and boulder samples from four study sites in Greenland. Uncertainties are 1σ. Information about AMS measurement standards, isotopic ratios, sample masses, and ICP-quantified total Al is reported in Supporting Information Table S3 for all samples. Details about the preparation and measurement of the 24 ^{10}Be analyses and the five previously-published ^{26}Al analyses, including ratios and blank corrections, are reported in the original publications containing the data. Information about background values for the new Al analyses is shown in Tables S4 and S5.

Figure Captions

Figure 1. Map of Greenland showing the locations of the four study sites.

Figure 2. Calculated ^{26}Al/^{10}Be ratios for each of the 23 bedrock and boulder samples (excluding one outlier). Error bars show ±1σ, with errors from the two individual isotopes propagated in quadrature. Samples are sorted by site along the x-axis.

Figure 3. York regression of ^{26}Al concentrations versus ^{10}Be concentrations (n = 23, excluding one outlier). Gray ellipses show samples' 1σ error for each of the two isotopes. Heavy dark line shows the uncertainty-weighted trendline through the dataset; thin dark lines show the 1σ uncertainty envelope around the trendline.

Sample Name	Study Site[a]	Sample Type	Latitude (°N)	Longitude (°E)	Elevation (m asl)	^{10}Be Conc. (x10^4 atoms g^{-1})	^{10}Be Unc. (x10^4 atoms g^{-1})	^{26}Al Conc. (x10^5 atoms g^{-1})	^{26}Al Unc. (x10^5 atoms g^{-1})	^{26}Al/^{10}Be Ratio	^{26}Al/^{10}Be Unc.	Predicted ^{26}Al/^{10}Be Ratio[b]
GT022	Thule	Boulder	76.55833	-68.19445	358	6.455	0.199	4.386	0.175	6.79	0.34	7.28
GT023	Thule	Boulder	76.56945	-68.24887	346	6.304	0.215	4.707	0.194	7.47	0.40	7.28
GT055	Thule	Boulder	76.56046	-68.54910	201	5.488	0.205	4.092	0.174	7.46	0.42	7.30
GU002	Upernavik	Boulder	72.53587	-53.73338	603	8.059	0.191	5.588	0.431	6.93	0.56	7.26
GU104	Upernavik	Bedrock	72.77333	-55.50288	253	6.025	0.117	4.314	0.551	7.16	0.92	7.29
GL003	Ilulissat	Bedrock	69.43373	-50.26645	395	4.734	0.120	3.342	0.222	7.06	0.50	7.28
GL004	Ilulissat	Boulder	69.43379	-50.26637	392	4.993	0.119	3.515	0.138	7.04	0.32	7.28
GL080	Ilulissat	Bedrock	69.39508	-50.41634	621	6.183	0.138	4.493	0.152	7.27	0.30	7.26
GL081	Ilulissat	Boulder	69.39530	-50.41563	618	6.010	0.113	4.858	0.227	8.08	0.41	7.26
GL088	Ilulissat	Bedrock	69.34380	-50.42943	95	3.493	0.105	2.942	0.137	8.42	0.47	7.30
GL089	Ilulissat	Boulder	69.34380	-50.42911	93	3.612	0.081	2.557	0.170	7.08	0.50	7.30
GL105	Ilulissat	Bedrock	69.29280	-50.60203	300	4.655	0.108	3.210	0.163	6.90	0.38	7.29
GL106	Ilulissat	Boulder	69.29280	-50.60203	300	4.576	0.094	3.339	0.129	7.30	0.32	7.29
GL107	Ilulissat	Bedrock	69.17960	-50.89068	53	3.663	0.081	2.676	0.147	7.30	0.43	7.30
GL108	Ilulissat	Boulder	69.17960	-50.89068	53	3.730	0.103	2.594	0.162	6.96	0.47	7.30
GLX14B	Narsarsuaq	Bedrock	61.29564	-45.57079	307	5.963	0.116	4.191	0.176	7.03	0.33	7.29
GLX16A	Narsarsuaq	Boulder	61.32355	-45.53717	467	6.964	0.137	5.417	0.202	7.78	0.33	7.27
GLX16B	Narsarsuaq	Bedrock	61.32281	-45.53704	469	7.267	0.141	5.361	0.160	7.38	0.26	7.27
GLX17A	Narsarsuaq	Boulder	61.33134	-45.54345	724	9.108	0.247	6.431	0.197	7.06	0.29	7.25
GLX17B	Narsarsuaq	Bedrock	61.33136	-45.54328	720	8.004	0.561	6.432	0.272	8.04	0.66	7.25
GLX25A[c]	Narsarsuaq	Boulder	61.19340	-45.30210	556	8.171	0.199	4.962	0.165	6.07	0.25	7.27
GLX25B	Narsarsuaq	Bedrock	61.19338	-45.30169	554	7.787	0.152	5.841	0.192	7.50	0.29	7.27
GLX28A	Narsarsuaq	Boulder	60.99539	-45.43148	52	4.709	0.196	3.931	0.253	8.35	0.64	7.30
GLX28B	Narsarsuaq	Bedrock	60.99537	-45.43146	50	4.667	0.119	3.681	0.172	7.89	0.42	7.30

[a]Previously-published data: Thule, Al and Be, *Corbett et al.* [2016] and *Corbett et al.* [2015]; Upernavik, Al and Be, *Corbett et al.* [2013]; Ilulissat, Be only, *Corbett et al.* [2011]; Narsarsuaq, Be only, *Nelson et al.* [2014].

[b]Predicted production ratios were calculated for each sample site using the CRONUScalc online calculator [*Marrero et al.* , 2016] and "SA" scaling [*Lifton et al.,* 2014].

[c]We treat this sample as an outlier (see text for details) and exclude it in our data analysis.

Figure 1.

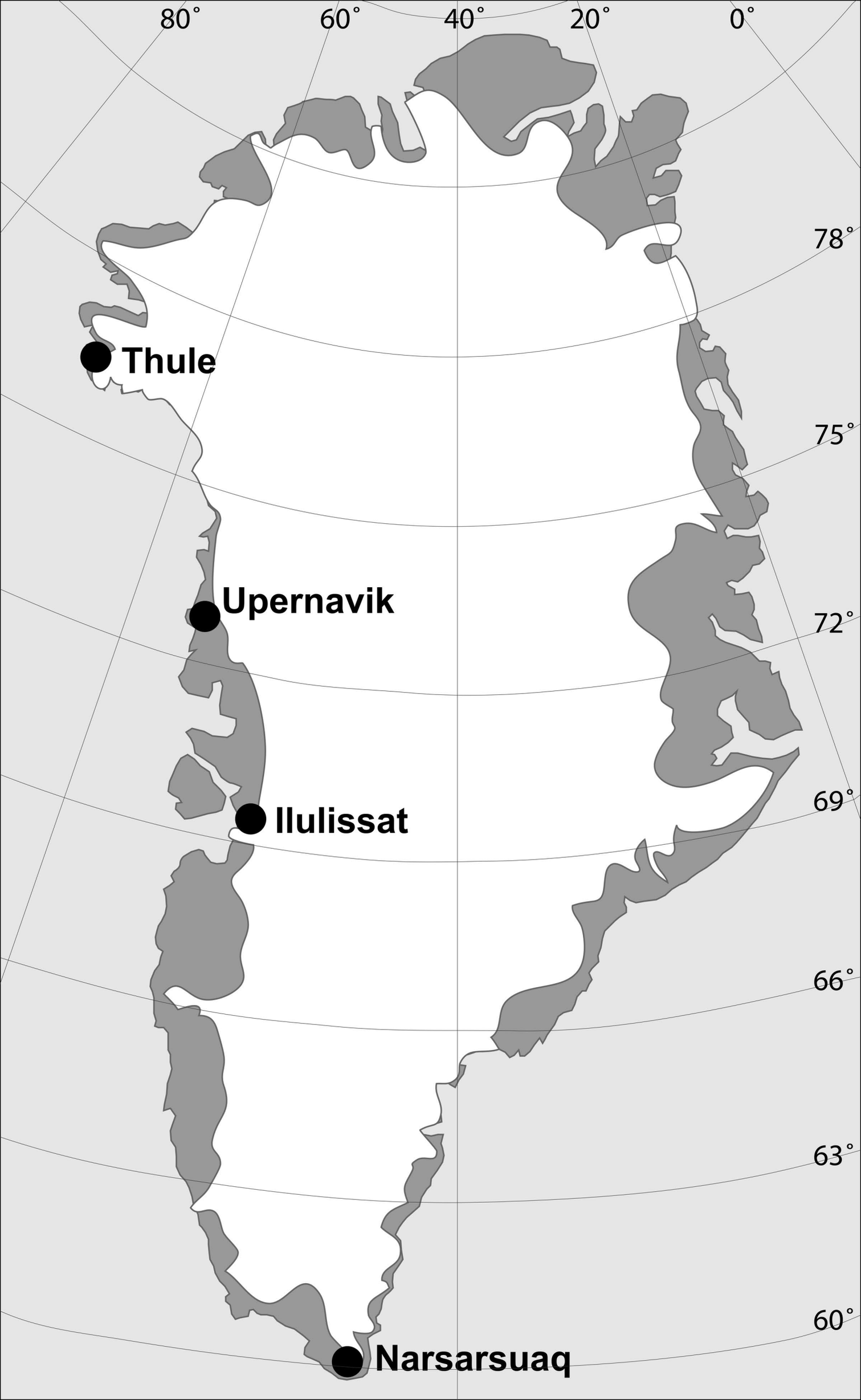
80°
60°
40°
20°
0°
78°
75°
72°
69°
66°
63°
60°
Thule
Upernavik
Ilulissat
Narsarsuaq

Figure 2.

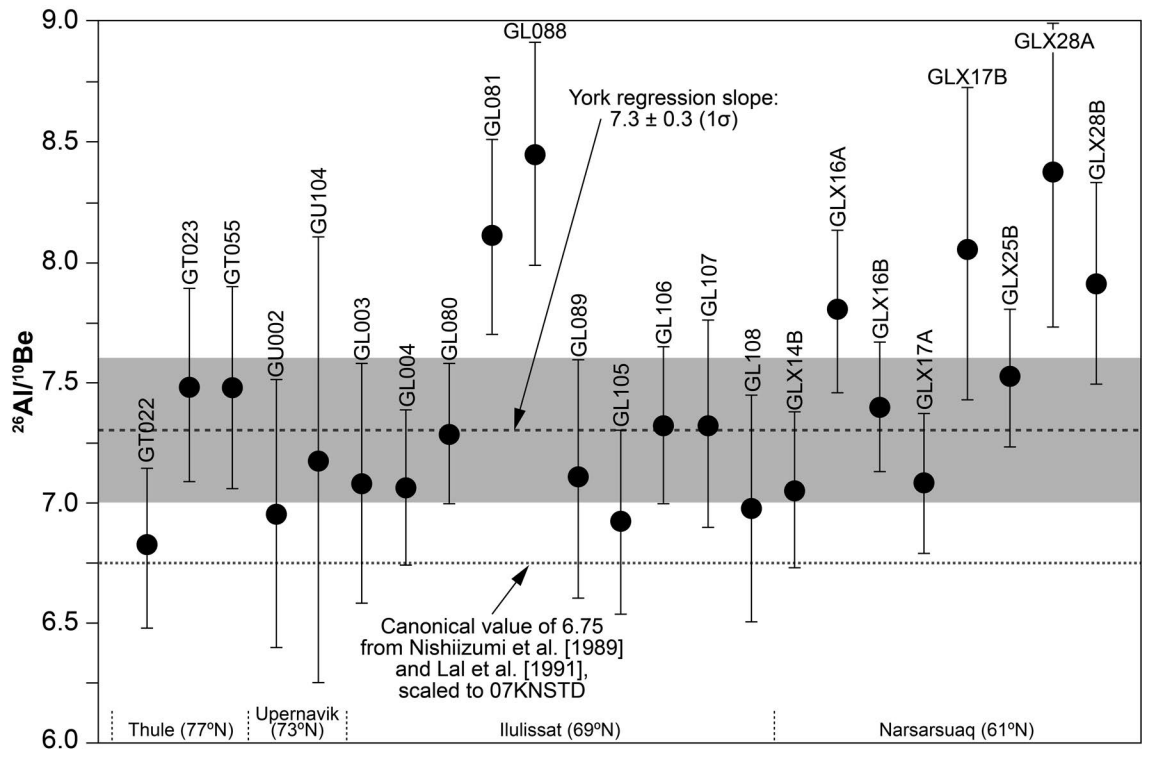
9.0
8.5
8.0
7.5
7.0
6.5
6.0
$^{26}Al/^{10}Be$
GT022
GT023
GT055
GU002
GU104
GL003
GL004
GL080
GL088
GL081
GL089
GL105
GL106
GL107
GL108
GLX14B
GLX16A
GLX16B
GLX17A
GLX17B
GLX25B
GLX28A
GLX28B
York regression slope:
7.3 ± 0.3 (1σ)
Canonical value of 6.75
from Nishiizumi et al. [1989]
and Lal et al. [1991],
scaled to 07KNSTD
Thule (77ºN)
Upernavik
(73ºN)
Ilulissat (69ºN)
Narsarsuaq (61ºN)

Figure 3.

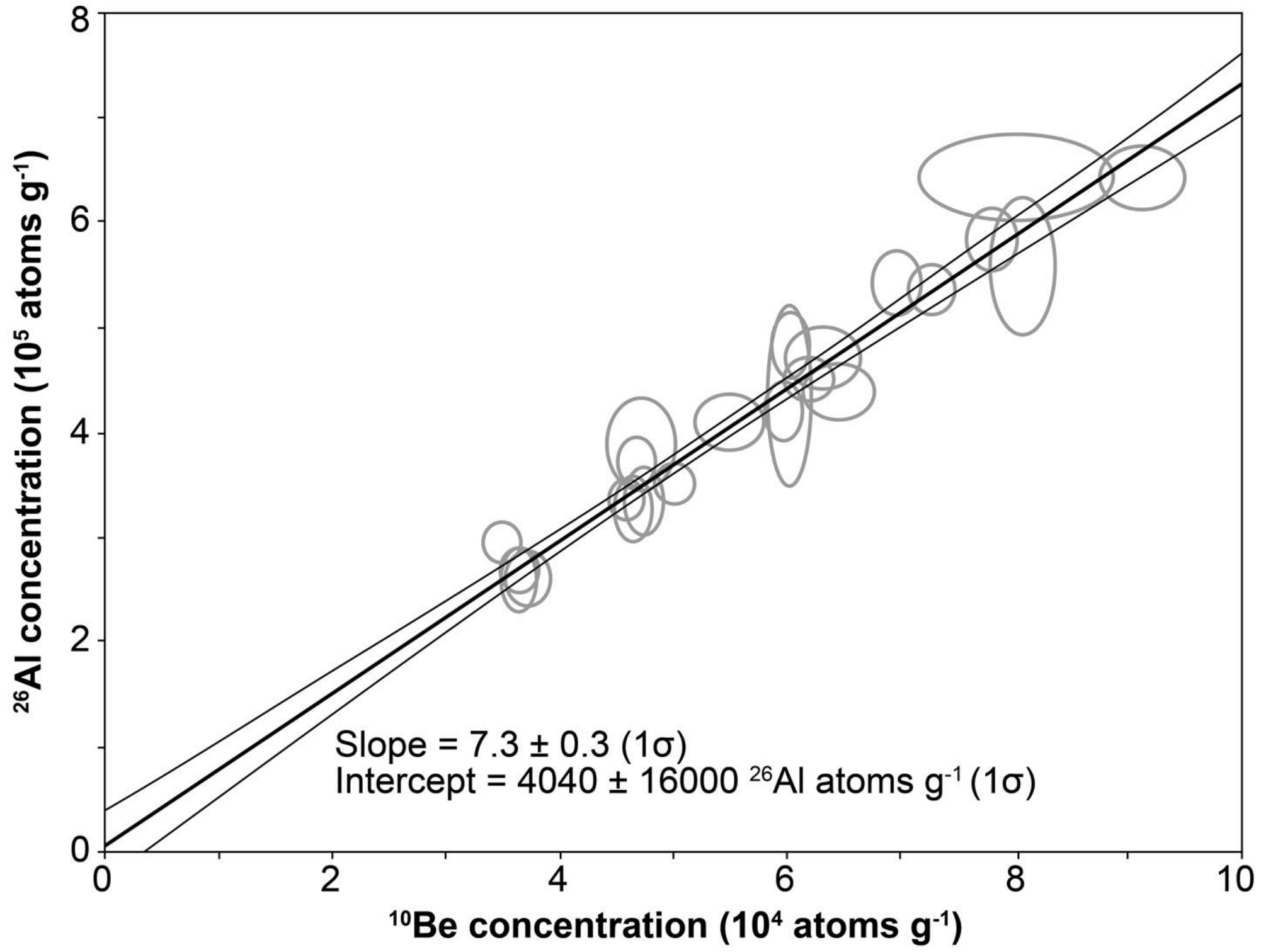
8
6
4
2
0
0
2
4
6
8
10
^{26}Al concentration (10^5 atoms g^{-1})
^{10}Be concentration (10^4 atoms g^{-1})
Slope = 7.3 ± 0.3 (1σ)
Intercept = 4040 ± 16000 ^{26}Al atoms g^{-1} (1σ)